Molecular Catalysis 470 (2019) 89–96

Contents lists available at ScienceDirect

Molecular Catalysis

journal homepage: www.elsevier.com/locate/mcat

Removal of groundwater nitrates by heterogeneous supramolecular complexes-like photocatalytic system based on in-situ generated and highly active Ti^{3+}/Ti^{2+} states in the reduced TiO_2

Dulanji S. Dharmagunawardhane[a], Nuwan L. De Silva[a], Udara Bimendra Gunatilake[a], Chang-Feng Yan[b], Jayasundera Bandara[a,*]

[a] National Institute of Fundamental Studies, Hantana Road, CP 20000, Kandy, Sri Lanka
[b] Hydrogen Production and Utilization Laboratory, Guangzhou Institute of Energy Conversion, Chinese Academy of Sciences, Guangzhou, 510640, China

ARTICLE INFO

Keywords:
Nitrate removal
Water treatments
Photocatalysis
Photoreduction
Reduced TiO
Ti^{3+}

ABSTRACT

In this investigation, a novel catalytic nitrate reduction method by using the in-situ generated Ti^{3+}/Ti^{2+} states in the TiO_2/Al catalyst was demonstrated. The Ti^{3+}/Ti^{2+} states in TiO_2/Al catalyst harvest the UV to near IR regions of the solar spectrum and continuously self-generated via the absorption of visible-near infrared radiations. The formation of reduced titanium oxidation states and the visible light harvesting properties of the catalyst were determined by X-ray Photoelectron Spectroscopy (XPS) analysis and diffuse reflectance transmission respectively. With the TiO_2/Al catalyst, over 95% of nitrate removal could be achieved for an initial nitrate concentration of 100 ppm. Based on XPS, FTIR analysis and the reaction products, a possible nitrate reduction mechanism is proposed in which in-situ generated Ti^{3+}/Ti^{2+} states can harvest visible-near infrared photons as well as found to be the active sites for the reduction of nitrates and hence function similar to supramolecular complex photocatalytic system. The catalytic system described can be easily adapted adapted for the groundwater nitrate removal.

1. Introduction

Nitrate is one of the most prevalent contaminants found in ground and surface water. According to the WHO and the Environmental Protection Agency (EPA) water quality standards, 10 ppm is the maximum contaminant level (MCL) for nitrate [1]. If the nitrate level exceeds the EPA maximum contamination level of 10 ppm in drinking water, it can pose a risk to human health. The excess nitrate in water originates from fertilizers, septic tanks, manure storage and sewage treatment methods as synthetic fertilizers and animal manure are rich in nitrogen [2]. On the other hand, the nitrogen-containing molecules in the soil are converted to nitrates by microbial activities, and move with the surface runoff into rivers and streams or leach into groundwater. It is known that the natural discharge from septic systems is one of the major contributors to the groundwater nitrate because septic systems remove only half of the nitrogen in wastewater, draining the remaining half to the groundwater. Hence, the wastewater discharge from the contemporary sewage treatment methods can pollute many water bodies and also the untreated sewage wastewater can enter the groundwater [3]. Presence of excessive nitrate in water can cause some serious health problems and it has been recommended that all infants, pregnant and nursing women should not drink the water that exceeds the nitrate level of 10 ppm [4]. Methemoglobinemia which is also called the blue baby syndrome is one of the major health problems related to excessive nitrate [5]. It also suspected that the high nitrate level in drinking water may increase the risk of cancer, disruption of thyroid function, diabetes, and birth defects [6]. Especially, N-Nitroso compounds produced in the human stomach by the ingested nitrite after reaction with organic compounds reported been highly carcinogenic to human [6].

Due to their adverse health effects, nitrates in ground and surface water have to be removed from the water sources to make it safe especially for drinking purpose and industrial uses. However, conventional water treatment methods are not effective in removing nitrates completely in water due to stability and high solubility of nitrate in water. Ion exchange [7,8], reverse osmosis (RO) [9,10], electrodialysis [11], photocatalysis/catalysis [12–17], biological [18,19], and chemical denitrification [20,21] methods have been employed effectively to remove nitrates in water. Due to the high operational cost, requirements of pre-treatment, inadequate nitrate removal efficiency, partial

* Corresponding author.
E-mail address: jayasundera.ba@nifs.ac.lk (J. Bandara).

https://doi.org/10.1016/j.mcat.2019.03.028
Received 14 November 2018; Received in revised form 6 March 2019; Accepted 26 March 2019

denitrification as well as the production of concentrated brine solution which required other waste disposal methods, most of above mentioned nitrate removal processes are not environmentally benign.

However, the photocatalytic removal of nitrate is more attractive since it provides a good substitute for the energy-intensive treatment methods. Yet the photocatalytic degradation systems based on high-bandgap semiconductors such as TiO_2, ZnO, $SrTiO_3$ are not sustainable methods due to poor harvesting of solar energy limiting their photocatalytic activity only to UV radiation [22,23]. Hence the development of visible light active photocatalysts is important for efficient harnessing of solar energy and practical application of photocatalysts in the remediation of environmental pollution [24–27]. Despite metal ion doping, co-sensitization, dye sensitization, composite semiconductors, anion doping and metal and metal ion implantation have been investigated to enhance the sustainability of photocatalysts, the present photocatalyic systems are not yet identified as a major pollution remediation technology [28–34]. In recent years, the black TiO_2 nanomaterial produced by the high-temperature hydrogenation of TiO_2 is an effective approach in shifting the bandgap of TiO_2 to around 1.5 eV and to harness the visible light [35–37]. The presence of Ti^{3+} states and oxygen vacancies in the black TiO_2 was proposed to be responsible for the extended light response [38–41]. The generation of catalytic active Ti^{3+} states and oxygen vacancies by the high-temperature hydrogenation process does not satisfy the green chemistry objectives. Additionally, highly reduced Ti^{3+} states are unstable and easily oxidized by air or dissolved oxygen in the water, which limits their practical applications [42,43].

Hence, in this study, highly stable and reduced Ti^{3+} and Ti^{2+} sites in TiO_2 particles were in-situ generated by the active Al-TiO_2 interaction which is an alternative to the high-temperature hydrogenation process. The proposed in-situ generation of active Ti^{3+} and Ti^{2+} sites in TiO_2 particles the active Al-TiO_2 interaction is rather a simple and environmentally friendly process. By using the TiO_2/Al photocatalyst, nitrate in water can be reduced efficiently and the presence of active catalytic Ti^{3+}/Ti^{2+} sites in TiO_2 was the origin of the observed enhanced catalytic activity of the reduced TiO_2. The interesting point in the TiO_2/Al photocatlytic system is the regeneracy and the in-situ generated Ti^{3+}/Ti^{2+} sites in TiO_2 particles act as both light harvesting as well as catalytic sites for the nitrate reduction reaction. Based on the XPS, FTIR analyses together with reaction products, a possible photocatalytic nitrate reduction mechanism is discussed. More importantly, the nitrate removal process described in this investigation is environmentally benign.

2. Experimental

2.1. Preparation of the catalyst

The TiO_2 coated Al-foil catalyst (hereafter TiO_2/Al) was prepared by spraying TiO_2 (Degussa P25) on the heated Al foil (0.1 mm, 99.96% purity) and sintering at 450 °C following the similar method described by Silva et.al [41]. For the preparation of the catalyst, the alumina sheet was cut into 2.5 cm × 15 cm size and cleaned with the detergent and washed with distilled water and ethanol to remove dirt on it. The TiO_2 solution made by mixing 500 mg of TiO_2, 15 µl of acetic acid (≥99.7 %, Fisher Scientific, Analar), 2 drops of Triton x-100 (Sigma Aldrich) in 50 ml of ethanol (≥99.8%, AnalaRNORMAPUR®) was magnetically stirred for 1 h at room temperature. The prepared TiO_2 suspension was sprayed on the heated alumina strip at a rate of 2 ml/min. The temperature of the Al-sheet was maintained at 200 °C during spray deposition of TiO_2 on the Al-sheet. Finally, the TiO_2 coated Al-foil strip was sintered at 450 °C for 3 h and allowed to cool slowly to prevent crack formation.

2.2. Characterization of the catalyst

Details of the catalyst characterization methods were given in SI. In brief, the crystalline structure of the catalyst was studied by using powder X-ray diffractometer. Surface morphology and cross-section of the catalyst were investigated by the field emission scanning electron microscope (FE-SEM, S-4800). Oxidation states of the catalyst were detected by XPS measurements. Light absorption was measured by using diffuse reflectance UV–vis spectroscopy. Reaction intermediates on the TiO_2 surface were analyzed by Fourier Transform Infrared spectroscopy (FTIR-8400S-Shimadzu, 4 cm^{-1}, resolution, 30 scans).

2.3. Photocatalytic activity of the catalyst

Nitrate reduction experiments were performed for a 100 mg/L of initial nitrate solution (potassium nitrate, 99.5%, KNO_3, BDH AnalaR®). For nitrate reduction reaction, a piece of TiO_2 coated Al substrate (2.5 cm × 15 cm area) that contained 75 mg of TiO_2 (2 mg of TiO_2 per 1 cm^2 of Al substrate) was employed. A TiO_2 coated glass plate (TiO_2/FTO) with the same dimension and the same amount of TiO_2 was used as the reference. For photocatalytic reaction, TiO_2/FTO and TiO_2/Al catalysts were dipped in the 100 ml of 100 mg/L of nitrate solution in separate reactors and nitrate reduction was carried out under UV–vis light irradiation, diffuse light irradiation and under dark condition. To determine the amount of nitrate, nitrite and ammonia present in the reaction solution, 10 ml portion of the solution was extracted after 1–6, 12, 22 and 24 h of reaction and nitrate, nitrite and ammonia were detected by colorimetric methods described in the supporting information. The long-term stability of the catalyst was performed by repeated use of the same catalyst for five consecutive days with three replicates. After 24 h use of the catalyst, a fresh 100 mg/L nitrate solution was introduced and the nitrate reduction was continued under similar irradiation conditions. The intensity of the light source was measured with a standard Si-reference cell (Newport).

3. Results and discussion

3.1. Characterization of the catalyst

The TiO_2/Al catalyst was characterized before and after nitrate reduction reactions. As shown in Fig. 1, the initial or as prepared TiO_2/Al catalyst absorbs light mainly below 400 nm by the transition of an electron from the valence band to the conduction band due to its high bandgap energy (~ 3.2 eV). However, within a few minutes of

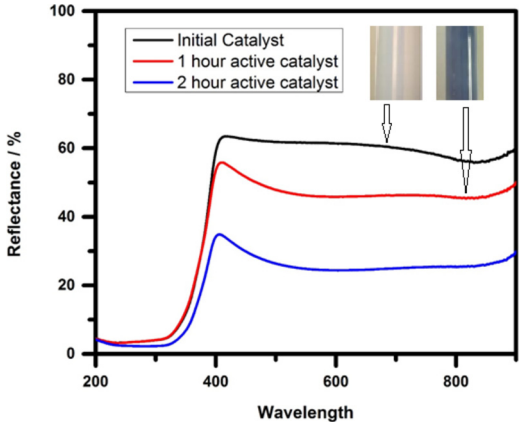

Fig. 1. The UV–vis DRS spectrum of TiO_2/Al (black), and TiO_2/Al catalyst after 60 (blue) and 120 (red) minutes irradiation with solar simulator respectively. Insets show the photograph of the initial and the 60 min irradiated TiO_2/Al catalyst. (For interpretation of the references to colour in this figure legend, the reader is referred to the web version of this article).

irradiation, the formation of blue colour was noticed in the TiO_2/Al catalyst and the intensity of the blue colour in the TiO_2/Al catalyst is deepen with the irradiation time (inset in Fig. 1). As shown in Fig. 1, with the concomitant formation of the blue colour in the catalyst, the light harvesting capability of the catalyst extends to Vis-near IR regions. It is known that the presence of reduced states such as Ti^{3+}/Ti^{2+} below the conduction band in the TiO_2 lattice is responsible for the formation of blue colour in TiO_2 and hence it can be assumed that the appearance of blue colour in the TiO_2/Al catalyst is due to the formation of reduced oxidation states such as Ti^{3+}/Ti^{2+} in the TiO_2 lattice of the TiO_2/Al catalyst [35,36,44,45].

These reduced states are found to be stable in air and the blue colour remains for several months. The formation of the blue colour of the TiO_2 is due to the presence of free electrons in the TiO_2 lattice and as a result, the reduced TiO_2 can harvest most of the visible light (Fig. 1). It is known that the mid-gap oxygen vacancies are generated in the TiO_2 lattice to maintain the electrostatic balance due to the formation of Ti^{3+} states in TiO_2 [38]. The electrons in these mid-gap states and shallow donor states get excited to the conduction band (CB) by the absorption of visible-NIR light yielding a blue colour in the reduced TiO_2 [46,47]. Especially, the absorption observed at 450–900 nm region, corresponds to 1.37–2.75 eV and such a shoulder absorption is characteristic of TiO_2 with mid-gap impurity states [41,48,49]. These reduced states of titanium play a significant role in enhancing the light harvesting capabilities of TiO_2 as well as its catalytic activity.

To confirm the formation of Ti^{3+}/Ti^{2+} states in TiO_2 (TiO_2/Al catalyst), XPS analysis was carried out and the XPS measurement of the TiO_2/Al catalyst which was taken after exposing TiO_2/Al to light for one hour is shown in Fig. 2a. For the comparison purpose, XPS measurement of TiO_2/FTO (TiO_2 coated on the FTO substrate) was also carried out and shown in Fig. 2b. The peaks at BEs of 458.2 eV and 464.0 eV in Fig.2b could be assigned to $2p_{3/2}$ and $2p_{1/2}$ peaks of Ti^{4+}−O of TiO_2 on the FTO substrate [50,51]. However, in the case of TiO_2/Al, $2p_{3/2}$ and $2p_{1/2}$ peaks were broadened and fitting results indicated that the $2p_{3/2}$ and $2p_{1/2}$ peaks of Ti^{4+}−O were shifted to 458.0 eV and 463.6 eV respectively. At the same time, in the broaden peak, two additional peaks could be easily identified as Ti^{3+}−O ($2p_{3/2}$ and $2p_{1/2}$ peaks at 457.6 and 456.2 eV respectively) and Ti^{2+}−O ($2p_{3/2}$ and $2p_{1/2}$ peaks at 457.6 and 456.2 eV respectively) confirming the formation of reduced Ti states in the TiO_2/Al catalyst [50,51]. Interestingly, no peak corresponding to Ti^{3+}−O was observed for TiO_2 in TiO_2/FTO indicating that the reduced Ti^{3+} is formed only in the TiO_2/Al catalyst.

The crystalline and surface morphology of the TiO_2/Al were investigated by XRD and SEM analyses respectively. The XRD patterns of the TiO_2/Al catalyst before (initial catalyst) and after 60 min of irradiation (reacted catalyst) are shown in Fig. 3 while the cross-sectional SEM images of the TiO_2/Al catalyst before and after 60 min of irradiation are shown in Fig. S1. As shown in Fig. 3, the diffraction patterns corresponding to both anatase and rutile TiO_2 could be identified in both the initial and the reacted TiO_2/Al samples. Diffraction peaks observed at 2θ at ca. 25° (101), 38° (004), 48° (220), 54° (105) and 55° (211) are due to anatase crystalline phase while the rutile crystalline phase has its characteristic peaks at ca. 27° (110), 36° (101), 41° (111) and 54° (211) (JCPDS 34–180) [52]. However, in the reacted TiO_2/Al samples (pH is not controlled during the reaction), a minor peak which corresponds to the AlOOH crystalline structure is clearly noticeable in addition to the standard anatase and rutile phase indicating the formation of AlOOH during nitrate reduction reaction. However, it was noted that the formation of AlOOH does not depend on the initial nitrate concentration indicating that Al is not consumed stoichiometrically during nitrate reduction reaction. Additionally, under the pH controlled nitrate reduction reaction, the formation of AlOOH is very greatly retarded indicating that the AlOOH formation is mainly relative with the change of the solution pH. The significance of this observation is that it confirms that the Al is not consumed stoichimoterically during the nitrate reduction reaction. The formation of AlOOH is also further evident by the cross-sectional SEM images shown in Fig. S1. The cross-sectional SEM image of the unreacted and the 48 h reacted TiO_2/Al catalysts are shown in Fig. S1a and b respectively. As shown in Fig. S1a, the TiO_2/Al catalyst contains roughly a ~ 30 μm thick TiO_2 layer on the Al substrate and a well defined crystalline TiO_2 nanoparticles were clearly noticeable. However, in the reacted TiO_2/Al catalyst, TiO_2 particles are partially covered with the AlOOH layer and we believe that the stability of the Ti^{+3} and Ti^{+2} could be due to the passivation of TiO_2 particles by the formation of a thin layer of AlOOH on TiO_2 particles. To confirm the passivation of Ti^{+3} and Ti^{+2} oxidation states in TiO_2 by the AlOOH layer, the EDS of the TiO_2/Al catalyst was carried out for the 48 h reacted sample and the mapping of Ti, Al and O distribution in the catalyst is shown in Fig. S1c. As shown in Fig. S1c, diffusion of AlOOH into the TiO_2 layer is clearly noticeable and these diffused AlOOH covered the TiO_2 nanoparticles which would lead to the passivation of Ti^{+3} and Ti^{+2} oxidation states in TiO_2. Interestingly, it was noted that by using the TiO_2/Al catalyst in the presence of visible light, the nitrates in the water can be effectively removed and in the following section the photocatalytic reduction of nitrates on the TiO_2/Al and TiO_2/FTO catalysts are discussed.

3.2. Photocatalytic nitrate reduction with the TiO_2/Al catalyst

The reduction of nitrate on the TiO_2/Al catalyst was carried out for 100 ppm nitrate solution under the UV–vis irradiation. For control reactions, the nitrate reduction reaction was also carried out with the Al substrate without TiO_2 under the same illumination condition and with the TiO_2/Al catalyst under the dark condition. As shown in Fig. 4, when the TiO_2/Al catalyst is irradiated with the UV–vis light (intensity of

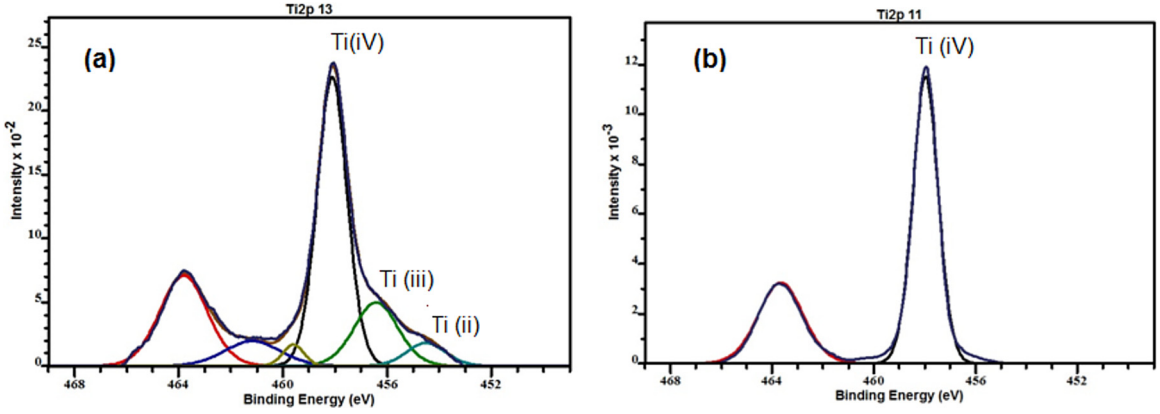

Fig. 2. The XPS measurements of (a) TiO_2/Al and (b) TiO_2/FTO catalysts taken after exposing them at light intensity of 100 mW/cm^2 at pH 6.5 in dist. H_2O for one h.

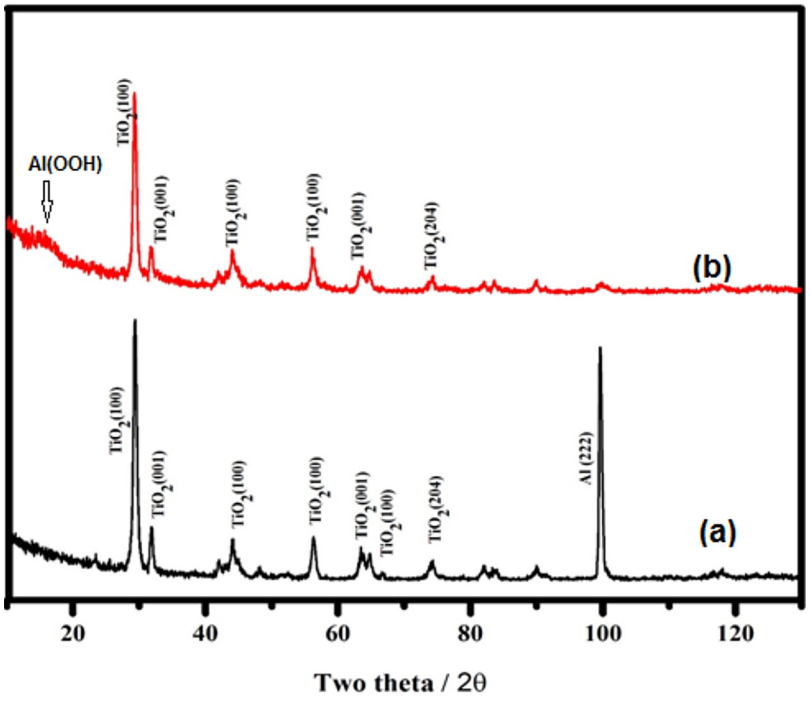

Fig. 3. XRD patterns of the TiO_2/Al catalyst, (a) before the reaction and (b) after 60 min of irradiation at light intensity of 100 mW/cm^2 at pH 6.5 in dist. H_2O.

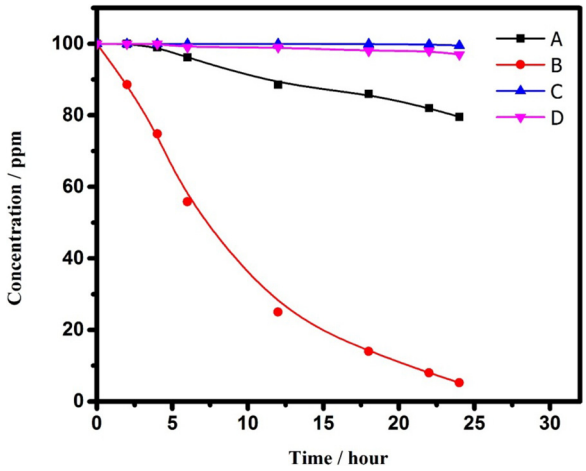

Fig. 4. Reduction of 100 ppm nitrate concentrate with time (A) TiO_2/FTO catalyst under irradiation (B) TiO_2/Al catalyst under irradiation of 100 mW/cm^2, (C) Al alone under light and (D) TiO_2/Al catalyst under dark. (The amount of TiO_2/Al catalyst is 2 mg of TiO_2 per 1 cm^2 of Al substrate2.5 cm × 15 cm area).

100 mW/cm^2), the concentration of the nitrate is decreased at a rate of 4.18 mg/L h^{-1} (rate constant of 0.114 h^{-1}) and over 99% nitrate removal was observed in 24 h of reaction. At the similar reaction condition, only 20% nitrate reduction was noted with the TiO_2/FTO catalyst. Also, no decrease in nitrate amount was noted when the reaction was carried out in dark condition (either with TiO_2/FTO and TiO_2/Al) or Al substrate alone (without TiO_2) under illumination. These results suggest the light initiated photocatalytic degradation of nitrate with the TiO_2/Al catalyst.

As described earlier, when the TiO_2/Al catalyst is exposed to light, $Ti^{3+/2+}$ states are generated in the TiO_2 and to check whether these $Ti^{3+/2+}$ states could reduce the nitrates, the reduction of nitrate reduction was carried out with the $Ti^{3+/2+}$ states containing blue coloured TiO_2/Al catalyst under dark condition as follows; the TiO_2/Al catalyst was pre-irradiated in water for 3 h to generate sufficient Ti^{+3} states in the TiO_2/Al (dark blue) catalyst and the pre-irradiated TiO_2/Al catalyst was immersed in 100 ppm nitrate solution and the reduction of nitrate concentration was measured under dark conditions. Interestingly, a decrease in nitrate concentration in solution was noted with the pre-irradiated TiO_2/Al (dark blue) catalyst under the dark condition at a rate of 2.13 mg/L h^{-1} confirming the participation of $Ti^{+3/+2}$ states in the degradation of nitrate reduction reaction. On the other hand, when the nitrate degradation was carried out under dark conditions with the initial TiO_2/Al sample that contains only Ti^{4+} states, nitrate degradation was not observed hence, it confirms that $Ti^{+3/+2}$ sites are responsible for the nitrate reduction reaction. Otherwise, the importance of this finding is that the $Ti^{+3/+2}$ states present in the pre-irradiated TiO_2/Al catalyst can be used for the in-situ treatment of groundwater nitrates by burying them under the soil as the active $Ti^{+3/+2}$ states generated in the pre-irradiated TiO_2/Al catalyst under light condition can reduce the ground water nitrates under no light condition. This process can be cycled by intermittent irradiation of the TiO_2/Al catalyst.

The dependence of the photocatalytic nitrate reduction rate on the initial nitrate concentrations was investigated and the results are shown in Fig. 5a. As shown in the inset in Fig. 5a, the plot of ln(C_0/C) versus reaction time (t) for different initial nitrate concentrations of (50–200 ppm) at optimal conditions of pH 5 and TiO_2/Al (2 mg of TiO_2 in 1 cm^2 Al, 2.5 × 15 cm^2 Al) yields a linear relationship, indicating the first-order kinetics for nitrate degradation. Furthermore, as shown in Fig. 5a, for the nitrate concentrations between 10–100 ppm nitrate and 75.0 mg of TiO_2 catalyst under one sun condition, a first-order reaction with a rate constant of ca. 0.002 min^{-1} can be clearly established. These kinetic data indicate that the reduction of nitrate with the TiO_2/Al catalyst at the reaction condition mentioned is not limited by the generation of charge carrier generation by the light reaction. To elucidate the effect of dosage of catalyst on the nitrate reduction reaction, nitrate reduction was carried out by varying the catalyst amount in the range 0.80–0.25 mg/l of TiO_2 catalyst at 100 ppm nitrate concentration (the TiO_2 amounts in the reaction medium was changed by taking different sizes of TiO_2/Al stripes for the reaction). A maximum concentration of 100 ppm was selected in this study as it was reported to be the upper limit of the contaminant nitrate level in the groundwater. The

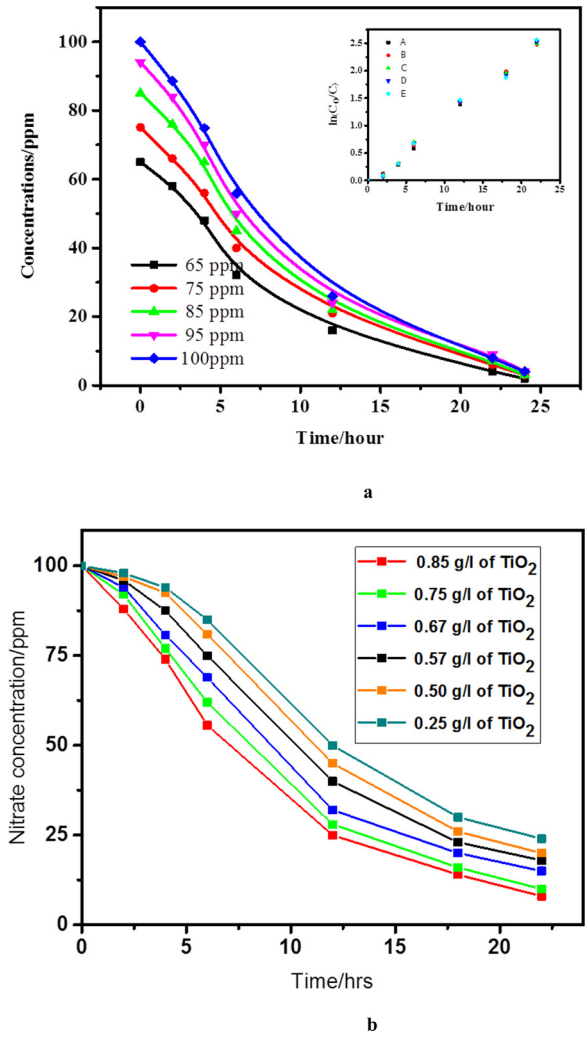

Fig. 5. (a) Reduction of nitrate with the variation of the initial nitrate concentration with the TiO_2/Al catalyst. The inset shows the plot of $\ln(C_0/C)$ versus reaction time (t). (The amount of TiO_2/Al catalyst is 2 mg of TiO_2 per 1 cm^2 of Al substrate2.5 cm × 15 cm area, light intensity of 100 mW/cm^2), (b) Reduction of nitrate with the variation of the amount of TiO_2/Al catalyst. The amount of TiO_2 was changed by varying the size of the Al strip. (The amount of TiO_2/Al catalyst is 2 mg of TiO_2 per 1 cm^2 of Al substrate, light intensity of 100 mW/cm^2).

dependence of catalyst dosage on the nitrate reduction is shown in Fig. 5b. As expected at a lower dosage of catalyst, the reaction is depended on the catalyst amount and hence the total number of active sites as the excited charge carrier generation is limited by the less number of active sites due to less amount of catalyst.

Additionally, the formation of hydrogen was noted with the concomitant nitrate reduction reaction when the TiO_2/Al catalyst was irradiated with 100 ppm nitrate solution. The hydrogen formation of the TiO_2/Al catalyst was investigated with the pure water and the nitrate solution and details of hydrogen analysis are given in SI. With the pure water and 100 ppm nitrate solution, 130 and 80 µl of hydrogen amounts were observed respectively after 2 h of irradiation of the TiO_2/Al catalyst at a light intensity of 100 mW/cm^2. The mechanism of nitrate reduction on the TiO_2/Al catalyst surface and the way the active hydrogen generated assists in the nitrate reduction reaction are discussed in section 2.3.

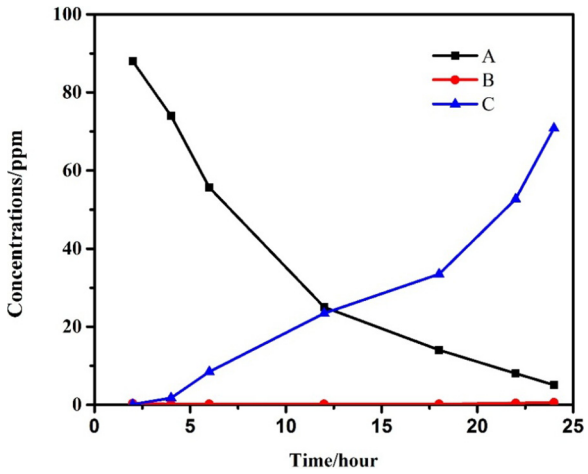

Fig. 6. Formation of nitrite and ammonia during nitrate reduction reaction with TiO_2/Al catalyst under irradiation; variation of concentrations of (A) nitrate, (B) nitrite and (C) ammonia with the reactions time.

3.3. Mechanism of the nitrate reduction reaction and the intermediate products

To establish the nitrate reduction path, expected reaction products in the nitrate reduction process such as nitrite and ammonia were monitored during the nitrate reduction reaction with the reaction time. As shown in Fig.6, with a lag time of two hours, both nitrite and ammonia formation was clearly observed. Also, with the decrease in nitrate concentrate, a concomitant increase in ammonia concentration can be observed while the nitrite concentration remains well below 1 ppm level. Furthermore, initially after 2 h of reaction, 2–3 ppm nitrite was noticed while the amount of ammonia was less than 0.1 ppm indicating that the nitrate is initially reduced to nitrite. The very low level of nitrite concentration during nitrate reduction reaction indicated that the nitrite is readily reacting on the TiO_2/Al catalyst. The observation that, when a 100 ppm nitrite solution was irradiated with the TiO_2/Al catalyst, the nitrite concentration in the solution was decreased rapidly with the formation of ammonia as the major product. The observed fast nitrite reduction kinetics on the TiO_2/Al catalyst is consistent with previous reports of nitrite and nitrate reduction kinetics [53]. Similarly, when a 100 ppm ammonia solution was irradiated with the TiO_2/Al catalyst, the formation of nitrate or nitrite was not observed but a slight decrease in ammonia concentration was noted. A slight decrease in ammonia concentration could be due to decomposition of ammonia or purged off the ammonia from the solution. It is known that the reduction of nitrate to nitrite involves two electrons, and the reduction of nitrite to ammonia involves six electrons [54]. Despite the reduction of nitrite to ammonia involves six electrons compared to two electrons in the reduction of nitrate to nitrite, the reduction of nitrate to nitrite is the rate determining step as it is a kinetically less favourable reaction [54]. Furthermore, the direct reduction of nitrate to ammonia is less favourable as it involves eight electrons. Hence, based on nitrate and nitrite degradation kinetics, it can be assumed that nitrate is first reduced to nitrite (a slow process) followed by the reduction of nitrite to ammonia (a fast process).

As the intermediate species identified in the solution during nitrate reduction reaction with the TiO_2/Al catalyst indicate that the nitrate is initially reduced to nitrite and then the nitrite is converted to ammonia, to identify the intermediate species formed on the catalyst surface and to investigate the nitrate reduction mechanism, FTIR study of the TiO_2/Al catalyst surface was carried out at different time intervals. The FTIR spectra of the TiO_2/Al catalyst before and after exposure to nitrate solution are shown in Fig. 7a and b respectively. In the FTIR spectra of the TiO_2/Al catalyst before exposure to nitrate solution (Fig. 7a), the

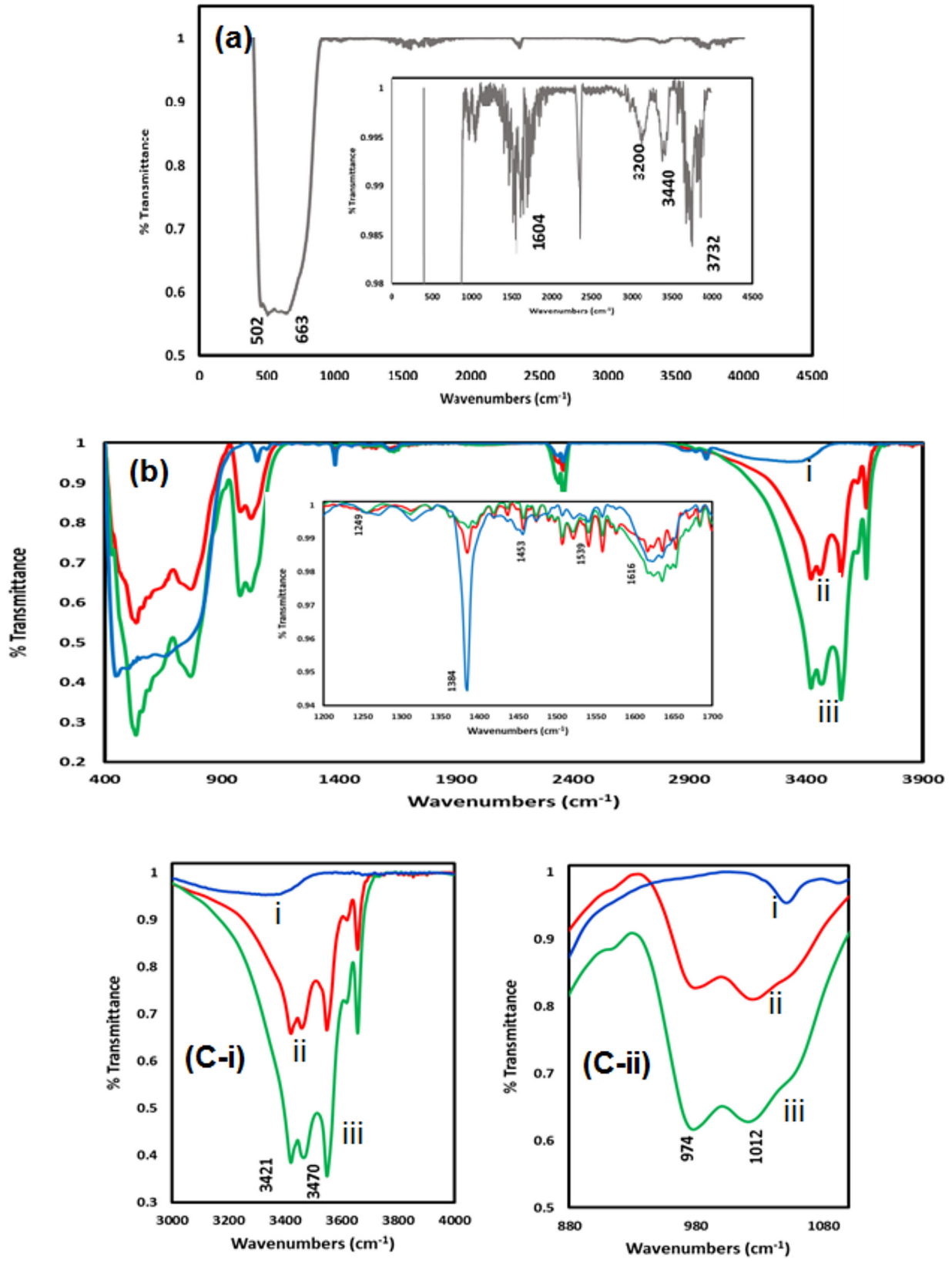

Fig. 7. FTIR spectra of (a) TiO_2/Al catalyst before expose to nitrate solution,(inset shows the expanded FTIR of the TiO_2/Al catalyst) (b) - i adsorbed nitrate on TiO_2/Al catalyst before irradiation, (b)-ii after irradiation for 6 h and (b)-iii after irradiation for 24 h. Inset in Fig. b shows the expanded FTIR to show the decrease in adsorbed nitrate peak at 1384 cm^{-1} with the reaction time and (c)-i and ii expanded FTIR spectra of Fig. 7b to show the increase in ammonia peaks with the reaction time.

Ti—O bridging peaks at 502 cm^{-1}, Ti—O non bridging peak at 663 cm^{-1}, OH bending at 1604 cm^{-1}, Ti—OH stretching 3200 cm^{-1}, and the OH/H_2O stretching vibrations at 3440 cm^{-1} can be identified [54,55]. When the nitrate solution was introduced to the TiO_2/Al catalyst, nitrates are adsorbed at the acid sites of TiO_2 by electrostatic interactions as a result of the reduction of the coordination number of terminal Ti^{4+} (presence of Ti^{3+} sites) leads to a positive charging of the surface. As shown in Fig. 7b and the inset in Fig. 7b, the bands at 1616, 1539 and 1249 cm^{-1} can be assigned to the N=O stretching mode of bidentate nitrate, Ti—O2NO and the bands at 1454 and 1384 cm^{-1} can be assigned to monodentate nitrate [54–57].

According to the FTIR results shown in Fig.7b, it can be clearly demonstrated that the intensity of the peak at 1385 cm^{-1} which is due to the stretching vibration of N—O (nitrate) decrease after 6 h of irradiation and almost diminished after 24 h because of the abatement of nitrate ions on the TiO_2/Al catalyst. Also it was noted the fast disappearance of monodentate nitrate than the bidentate nitrates. As shown in Fig. 7b, with the disappearance of nitrate IR bands on the TiO_2 surface, concomitant appearance of strong IR bands that are corresponding to ammonia was noted. For clarity of presentation, the expanded FTIR spectra of Fig. 7b in the 3000–4000 cm^{-1} and 880–1080 cm^{-1} are shown in Fig. 7C-i and C-ii respectively. As shown in Fig. 7b and c, the sharp peaks at 3470 cm^{-1} and 3421 cm^{-1} located in the regions of 3400–3100 cm^{-1} can be ascribed to N—H stretching vibration of coordinated ammonium ions [58]. Additional bands seen at 1012 and 974 cm^{-1} also can be attributed to ammonium ion coordinated at Lewis acid sites. As shown in Fig. 7b and c, the gradual increase of the intensity of bands due to ammonia with concomitant decrease in the intensity of nitrate band is a clear evidence that nitrate is converted to ammonia with the irradiation time. Despite nitrite was detected in nitrate reduction solution, IR bands due to nitrite is not clearly distinguishable on the TiO_2/Al catalyst surface which could be probably due to the fast conversion of nitrite into ammonia as described in photocatalytic degradation of nitrite in section 3.2. On the other hand, nitrate and ammonia amounts are higher than the amount of nitrate on the TiO_2 surface and hence strong IR responses due to nitrate and ammonia may overlap the weak IR bands of nitrite. On the other hand, strong IR response of nitrate and ammonia (the concentrations of ammonia and nitrate are much higher than the nitrite concentration) may overlap the weak IR bands of nitrite.

With these obtained results, a possible reaction pathway for the nitrate reduction is given in Reactions (1–8) and schematically shown in Fig. 8. As the first step of nitrate reduction on the TiO_2/Al catalyst, nitrate molecules formed bidentate (mainly) or monodentate (minor) chelating adsorbed species on the TiO_2 surface (Reaction 1). Once nitrates are adsorbed on the surface of TiO_2/Al catalyst, the nitrates are then reduced by the electron enriched titania species probably by Ti^{3+}/Ti^{2+} sites generated via the Reaction (2)leading to the formation of nitrites (Reaction 3). In the process of catalytic nitrate reduction process on the TiO_2/Al catalyst, the reduce Ti^{3+} sites act as both light harvesting sites and catalytic sites. On the other hand, it is known that these reduce Ti^{3+}/Ti^{2+} states capture excited charge carriers and react with H^+ generating active H^o (Reaction 4) and these active H^o can be combined to form H_2 (Reaction 5) [41]. The active H^o readily reacts with nitrites formed by the Reaction (3) and the nitrite is rapidly reduced to the ammonium ion (Reaction 6). The active Ti sites can be regenerated by leaving the NH_3 formed on the TiO_2 surface.

In the photocatalytic nitrate degradation process described, nitrates are first reduced to nitrite and then to ammonia and the rate determining step is the reduction of nitrate to nitrite. Formation of active H^o by the Ti^{3+} states may accelerate or facilitate the nitrate reduction reaction. As described earlier, the lower hydrogen yield with nitrate solution than the pure water could be due to the consumption of generated hydrogen in the nitrate reduction reactions as given in Reactions (1)–(8). Additionally, holes can react with adsorbed OH species or Al generating OH radicals or Al^{3+} species respectively as given in Reactions (7) and (8). The reported novel nitrate reduction method in this investigation by the in-situ generated reduced $Ti^{3+/2+}$ species is a simple, effective and low cost method to treat nitrate in water.

$$TiO_2 \equiv +NO_3^-(sol) \rightarrow TiO_2 \equiv -NO_3^-(ads) \quad (TiO_2 \equiv \text{surface of } TiO_2) \tag{1}$$

$$TiO_2/Al + h\nu \rightarrow e^- + h^+ \tag{2}$$

$$TiO_2 \equiv {}^{-}NO_3{}^{-}(ads) + 2e^- + H_2O \rightarrow TiO_2 \equiv -NO_2{}^{-}(ads) + 2OH^- \tag{3}$$

$$e^- + H^+ \rightarrow \text{active } H^o \tag{4}$$

$$H^o + H^o \rightarrow H_2 \tag{5}$$

$$TiO_2 \equiv -NO_2{}^{-}(ads) + 6e^- + 7H^+ \rightarrow TiO_2 \equiv -NH_3(ads) + 2H_2O \tag{6}$$

$$h^+ + OH \rightarrow OH^o \tag{7}$$

$$3h^+ + Al \rightarrow Al^{3+} \tag{8}$$

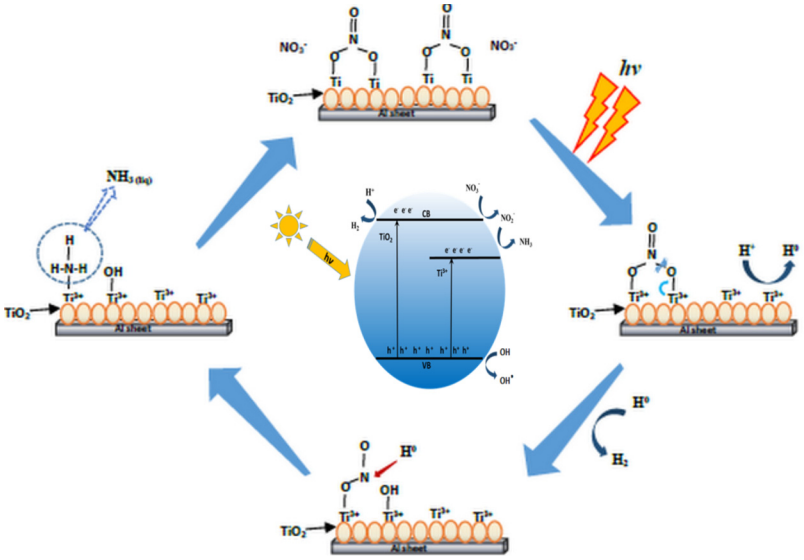

Fig. 8. Schematic presentation of the proposed nitrate reduction path and the intermediate formation mechanism.

These results clearly demonstrate that the in-situ generated Ti^{3+} and Ti^{2+} sites in TiO_2 particles by the active Al-TiO_2 interaction can degrade nitrate efficiently and based on the reaction products a possible photocatalytic nitrate reduction mechanism was discussed.

4. Conclusions

Nitrates in water and especially groundwater can be removed efficiently by the in-situ generated Ti^{3+} and Ti^{2+} sites in TiO_2 particles. The generation of Ti^{3+} and Ti^{2+} sites in TiO_2 particles by the active Al-TiO_2 interaction is an alternative to the high-temperature Ti^{3+} and Ti^{2+} generation by the hydrogenation process. In-situ generated, Ti^{3+} and Ti^{2+} sites in TiO_2 particles by the active Al-TiO_2 interaction are found to be highly stable. The TiO_2/Al catalyst is found to be active in the Vis-near IR regions of the solar spectrum and the active sites of the catalyst are the reduced $Ti^{3+}$and Ti^{2+} states in the TiO_2 lattice. In the photocatalytic nitrate degradation process, nitrates are first reduced to nitrite and then to ammonia and the rate determining step is the reduction of nitrate to nitrite. Formation of active H^o by the Ti^{3+} states may accelerate or facilitate the nitrate reduction reaction. The novel nitrate degradation method reported in this investigation can be employed to treat the nitrate-contaminated water effectively as it is simple, effective and low cost. More importantly, the nitrate removal processes described in this investigation is environmentally benign.

Conflicts of interest

There are no conflicts to declare.

Acknowledgement

JB would like to acknowledge the Chinese Academy of Sciences for CAS PIFI fellowship offered to him to conduct this research. Authors would like to thank D. Aluthpatabendi for photocatalytic experiment. Financial support from the National Natural Science Foundation of China (No. 51576201) is highly appreciated.

Appendix A. Supplementary data

Supplementary material related to this article can be found, in the online version, at doi:https://doi.org/10.1016/j.mcat.2019.03.028.

References

[1] The world health report 1996 - Fighting disease, fostering development, https://www.who.int/whr/1996/en/.
[2] D.S. Powlson, T.M. Addiscott, N. Benjamin, K.G. Cassman, T.M. de Kok, H. van Grinsven, J.-L. L'hirondel, A.A. Avery, C. Van Kessel, J. Environ. Qual. 37 (2008) 291–295.
[3] F.T. Wakida, D.N. Lerner, Water Res. 39 (2005) 3–16.
[4] L. Knobeloch, B. Salna, A. Hogan, J. Postle, H. Anderson, Environ. Health Perspect. 108 (2000) 675.
[5] D.R. Lewis, Am. Indian Q. 19 (1995) 423–450.
[6] F. Maqbool, S. Mostafalou, H. Bahadar, M. Abdollahi, Life Sci. 145 (2016) 265–273.
[7] L.P. Mazur, M.A.P. Cechinel, S.M.A.G.U. de Souza, R.A.R. Boaventura, V.J.P. Vilar, J. Environ. Manage. 223 (2018) 215–253.
[8] M. Lawrinenko, D.A. Laird, Green Chem. 17 (2015) 4628–4636.
[9] L. Malaeb, G.M. Ayoub, Desalination 267 (2011) 1–8.
[10] R. Epsztein, O. Nir, O. Lahav, M. Green, Chem. Eng. J. 279 (2015) 372–378.
[11] B. Van der Bruggen, A. Koninckx, C. Vandecasteele, Water Res. 38 (2004) 1347–1353.
[12] R. Lucchetti, L. Onotri, L. Clarizia, F. Di Natale, I. Di Somma, R. Andreozzi, R. Marotta, Appl. Catal. B: Environ. 202 (2017) 539–549.
[13] J. Bandara, J. Kiwi, C. Pulgarin, P. Peringer, G.-M. Pajonk, A. Elaloui, P. Albers, Environ. Sci. Technol. 30 (1996) 1261–1267.
[14] S. Zhang, X. Lu, Chemosphere 206 (2018) 777–783.
[15] J. Sá, T. Berger, K. Föttinger, A. Riss, J.A. Anderson, H. Vinek, J. Catal. 234 (2005) 282–291.
[16] Z. Liu, H. Liu, X. Feng, L. Ma, X. Cao, B. Wang, Mol. Catal. 445 (2018) 179–186.
[17] T. Boningari, S.M. Pavani, P.R. Ettireddy, S.S.C. Chuang, P.G. Smirniotis, Mol. Catal. 451 (2018) 33–42.
[18] J.Y. Park, Y.J. Yoo, Appl. Microbiol. Biotechnol. 82 (2009) 415–429.
[19] D. Patureau, N. Bernet, T. Bouchez, P. Dabert, J.P. Delgenes, R. Moletta, J. Mol. Catal. B Enzym. 5 (1998) 435–439.
[20] A.E. Palomares, J.G. Prato, F. Rey, A. Corma, J. Catal. 221 (2004) 62–66.
[21] U. Prüsse, K.-D. Vorlop, J. Mol. Catal. A Chem. 173 (2001) 313–328.
[22] L.G. Devi, R. Kavitha, Appl. Catal. B: Environ. 140-141 (2013) 559–587.
[23] J. Jing, M. Liu, V.L. Colvin, W. Li, W.W. Yu, J. Mol. Catal. A Chem. 351 (2011) 17–28.
[24] N. Zhang, M.-Q. Yang, S. Liu, Y. Sun, Y.-J. Xu, Chem. Rev. 115 (2015) 10307–10377.
[25] X. Pan, Y.-J. Xu, J. Phys. Chem. C 117 (2013) 17996–18005.
[26] K. Tennakone, J. Bandara, Sol. Energy Mater. Sol. Cells 60 (2000) 361–365.
[27] A. Gannoruwa, B. Ariyasinghe, J. Bandara, Catal. Sci. Technol. 6 (2016) 479–487.
[28] M. Pelaez, N.T. Nolan, S.C. Pillai, M.K. Seery, P. Falaras, A.G. Kontos, P.S.M. Dunlop, J.W.J. Hamilton, J.A. Byrne, K. O'Shea, M.H. Entezari, D.D. Dionysiou, Appl. Catal. B: Environ. 125 (2012) 331–349.
[29] T. Ihara, M. Miyoshi, Y. Iriyama, O. Matsumoto, S. Sugihara, Appl. Catal. B: Environ. 42 (2003) 403–409.
[30] K. Kulathunga, A. Gannoruwa, J. Bandara, Catal. Commun. 86 (2016) 9–13.
[31] K. Vinodgopal, D.E. Wynkoop, P.V. Kamat, Environ. Sci. Technol. 30 (1996) 1660–1666.
[32] S. Rehman, R. Ullah, A.M. Butt, N.D. Gohar, J. Hazard. Mater. 170 (2009) 560–569.
[33] Y. Huang, Y. Gao, Q. Zhang, Y. Zhang, J.-j. Cao, W. Ho, S.C. Lee, J. Hazard. Mater. 354 (2018) 54–62.
[34] J. Chen, F. Qiu, W. Xu, S. Cao, H. Zhu, Appl. Catal. A 495 (2015) 131–140.
[35] X. Chen, L. Liu, F. Huang, Chem. Soc. Rev. 44 (2015) 1861–1885.
[36] M. Tian, M. Mahjouri-Samani, G. Eres, R. Sachan, M. Yoon, M.F. Chisholm, K. Wang, A.A. Puretzky, C.M. Rouleau, D.B. Geohegan, ACS Nano 9 (2015) 10482–10488.
[37] I. Nakamura, N. Negishi, S. Kutsuna, T. Ihara, S. Sugihara, K. Takeuchi, J. Mol. Catal. A Chem. 161 (2000) 205–212.
[38] Y. Zhou, C. Chen, N. Wang, Y. Li, H. Ding, J. Phys. Chem. C 120 (2016) 6116–6124.
[39] S.G. Ullattil, S.B. Narendranath, S.C. Pillai, P. Periyat, Chem. Eng. J. 343 (2018) 708–736.
[40] L. Han, B. Su, G. Liu, Z. Ma, X. An, Mol. Catal. 456 (2018) 96–101.
[41] N.L. De Silva, A. Jayasundera, A. Folger, O. Kasian, S. Zhang, C.-F. Yan, C. Scheu, J. Bandara, Catal. Sci. Technol. 8 (2018) 4657–4664.
[42] Z. Wang, B. Wen, Q. Hao, L.-M. Liu, C. Zhou, X. Mao, X. Lang, W.-J. Yin, D. Dai, A. Selloni, J. Am. Chem. Soc. 137 (2015) 9146–9152.
[43] T.L. Thompson, J.T. Yates, Chem. Rev. 106 (2006) 4428–4453.
[44] A. Naldoni, M. Allieta, S. Santangelo, M. Marelli, F. Fabbri, S. Cappelli, C.L. Bianchi, R. Psaro, V. Dal Santo, J. Am. Chem. Soc. 134 (2012) 7600–7603.
[45] C. Zhu, J. Zheng, L. Fang, P. Hu, Y. Liu, X. Cao, M. Wu, J. Mol. Catal. A Chem. 424 (2016) 135–144.
[46] D. Payne, Y. Zhang, C. Pang, H. Fielding, G. Thornton, Top. Catal. 60 (2017) 392–400.
[47] X. Pan, M.-Q. Yang, X. Fu, N. Zhang, Y.-J. Xu, Nanoscale 5 (2013) 3601–3614.
[48] X. Chen, L. Liu, P.Y. Yu, S.S. Mao, Science 331 (2011) 746–750.
[49] S. Nishanthi, E. Subramanian, B. Sundarakannan, D.P. Padiyan, Sol. Energy Mater. Sol. Cells 132 (2015) 204–209.
[50] B.V. Crist, D.B. Crisst, Handbook of Monochromatic XPS Spectra, Wiley, New York, 2000.
[51] A.F. Carley, P.R. Chalker, J.C. Riviere, M.W. Roberts, J. Chem. Soc. Faraday Trans. Phys. Chem. Condensed Phases 83 (1987) 351–370.
[52] J.F. Porter, Y.-G. Li, C.K. Chan, J. Mater. Sci. 34 (1999) 1523–1531.
[53] M.J. Alowitz, M.M. Scherer, Environ. Sci. Technol. 36 (2002) 299–306.
[54] E. Pérez-Gallent, M.C. Figueiredo, I. Katsounaros, M.T. Koper, Electrochim. Acta 227 (2017) 77–84.
[55] J. Sa, J.A. Anderson, Appl. Catal. B: Environ. 77 (2008) 409–417.
[56] M. Kantcheva, J. Catal. 204 (2001) 479–494.
[57] J. Navio, M. Macias, A. Justo, C. Real, J. Therm. Anal. Calorim. 38 (1992) 673–682.
[58] F. Liu, H. He, C. Zhang, W. Shan, X. Shi, Catal. Today 175 (2011) 18–25.